IEEE Robotics and Automation Letters (RA-L) paper, presented at ICRA 2024, Yokohama, Japan. Cite as RA-L paper.

Adaptive Active Disturbance Rejection Control of An Actuated Ankle Foot Orthosis for Ankle Movement Assistance

R. Jradi, H. Rifaï, S. Mohammed

***Abstract*—Foot-drop (FD) is a post-stroke gait disorder characterized by impaired foot lifting during the swing phase. This paper focuses on providing a continuous ankle joint assistance throughout the gait cycle using an actuated ankle foot orthosis (AAFO). The control strategy is based on an adaptive active disturbance rejection controller (AADRC) such that the orthosis provides the only required amount of assistance to complement the human effort needed to perform the walking activity. The proposed controller exhibits adaptability, making it suitable for various subjects without the need for prior parameter identification. To demonstrate its effectiveness, the control strategy is experimentally validated with five healthy subjects and compared to state-of-the-art controllers.**

***Index Terms*—Robust/Adaptive Control, Wearable Robotics, Prosthetics and Exoskeletons, Rehabilitation Robotics.**

I. Introduction

ACCORDING to the World Health Organization (WHO), approximately 15 million people worldwide experience strokes annually, with 30 % of them being left with disabilities. Stroke is recognized as one of the leading causes of disability, as it can significantly impact the movement of the limbs in the human body. It is important to highlight that a substantial proportion (20-30%) of post-stroke patients are at risk of developing foot-drop (FD) which highly impacts their quality of life [1]. FD patients exhibit a weakness in the dorsiflexor muscles of the ankle joint, resulting in their inability to lift the foot during the swing phase of the gait cycle or dorsiflex the ankle joint upon foot landing (initial contact event). This weakness significantly compromises walking stability and increases the risk of fall.

Conventional therapy offers a solution by emphasizing exercises that aim to strengthen specific muscles. However, this approach typically necessitates high-intensity and repetitive training, which significantly relies on the expertise of the therapist [2]. Assistive devices like Ankle Foot Orthoses (AFO) play a crucial role in preventing foot dragging during the swing phase of the gait cycle [3]. Existing passive AFO designs either force the ankle joint into a fixed 90° orientation [4] or provide passive support through the use of springs and dampers [5]. Actuated Ankle Foot Orthoses (AAFOs) offer a robotic-based solution that provides controlled assistance in both dorsiflexion and plantarflexion directions, enabling the wearer to achieve a more natural gait. By externally actuating the ankle joint, AAFOs offer improved controllability and a greater range of motion compared to passive AFOs.

Three main types of AAFO controllers have been mainly investigated in the literature. EMG-based controllers for AAFOs utilize measured muscular activity to generate a proportional assistive torque [6]. However, implementing these strategies in practice can be challenging due to the influence of sensor placement and skin condition on the accuracy and reliability of EMG signals. Impedance-based control has found extensive application in AAFOs, involving the adjustment of mechanical properties within the orthosis-wearer system based on the detected gait events. While these controllers are effective, they rely on the wearer's minimal residual effort to initiate movement. Another frequently used strategy is the trajectory tracking controllers, wherein the orthosis tracks a predefined ankle joint trajectory [7]–[11]. These controllers have the capability to offer corrective assistance without relying on the residual human effort. However, the tuning of the above-mentioned controller type often depends on the estimated AAFO-wearer parameters. Therefore, an identification process needs to be performed prior to each rehabilitation session, which is time and effort consuming. Note that the identified parameters during a given session may also change with respect to the gait sub-phases or due to some external factors like muscular fatigue. The adaptive approach proposed in this paper attempts to address both the parameter and the human muscular effort variations. It is based on an adaptive active disturbance rejection controller (AADRC). This controller combines two main features: 1) an adaptive extended state observer (AESO) that estimates the human muscular torque and the unmodelled dynamics and 2) an adaptive model reference control torque that allows to ensure an accurate tracking of an adaptive desired ankle joint trajectory. By estimating and compensating the human muscular torque, the controller provides only the required amount of assistance needed to perform a movement in complement of the human effort. Moreover, due to the adaptability of the estimator/controller parameters, the AADRC strategy is suitable to different wearer profiles without the need of prior parameter identification process. Besides, it can adapt to any change in the human muscular torque or parameter/dynamics of the AAFO-wearer system during the same session. The time varying gains will additionally reduce the impact of measurement noise on the state estimation and accelerate the convergence speed [12].

Manuscript received: July 14, 2023; Revised: September 30, 2023 ; Accepted: October 17, 2023.

This paper was recommended for publication by Editor Clement Gosselin upon evaluation of the Associate Editor and Reviewers' comments.

R. Jradi, H. Rifaï and S. Mohammed are with Univ Paris Est Creteil, LISSI, F-94400 Vitry, France {rami.jradi, hala.rifai, samer.mohammed}@u-pec.fr

Digital Object Identifier (DOI): see top of this page.

IEEE Robotics and Automation Letters (RA-L) paper, presented at ICRA 2024, Yokohama, Japan. Cite as RA-L paper.

IEEE Robotics and Automation Letters (RA-L) paper, presented at ICRA 2024, Yokohama, Japan. Cite as RA-L paper.

Active disturbance rejection controllers (ADRC) have been developed for lower limb exoskeleton control [10], [13], [14]. The proposed controller provides the benefit of not requiring a prior parameter identification process and the ability to adapt to variations in parameters or external torque.

The rest of this paper is organized as follows. In Section II, the model of the AAFO-wearer system is presented. Section III provides a detailed explanation of the adaptive active disturbance rejection control strategy. The simulations and experimental results are presented in Section IV. Finally, Section V concludes the paper and discusses future directions.

II. AAFO-Wearer System Modeling

The orthosis used in this study is attached to the left leg by means of straps that secure it around the calf and thigh (Fig. 1). It consists of one passive degree of freedom (DoF) at the knee joint and an active DoF at the ankle joint. The foot and the orthosis together constitute a rigid body known as the AAFO-wearer system. To effectively model this system, three primary frames are defined, as illustrated in Fig. 1e. The global frame, $G(\vec{x}^g, \vec{y}^g, \vec{z}^g)$, where the $\vec{x}_g$ and $\vec{y}_g$ axes are respectively parallel and perpendicular to the walking direction, the shank frame, $S(\vec{x}^s, \vec{y}^s, \vec{z}^s)$ where its $\vec{y}_s$ axis is fixed to the shank of the AFO-wearer system and the corresponding $\vec{x}_s$ axis is perpendicular to $\vec{y}_s$ and oriented in the walking direction. The foot frame, $F(\vec{x}^f, \vec{y}^f, \vec{z}^f)$ is attached to the foot of the wearer at the ankle joint level, its $\vec{x}_f$ axis is parallel to the foot. The corresponding z axis of each frame is obtained such that the three-sided frame is direct. All three frames have the ankle joint as origin.

Let θ designate the ankle joint angle, which is defined as the angle between the vectors $\vec{x}_s$ and $\vec{x}_f$. The shank inclination angle θ_s is the angle between the vertical axis $\vec{y}_g$ and the shank axis $\vec{y}_s$. The angle α is the foot inclination and is considered between $\vec{x}_g$ and $\vec{x}_f$. The angles θ and θ_s are measured respectively through the use of an incremental encoder integrated into the orthosis and a wearable Inertial Measurement Unit (IMU) positioned on the shank. The angle α can be obtained using the following: $\alpha = \theta + \theta_s$.

Due to the presence of multiple torques acting on the AAFO-wearer system, its dynamics can be mathematically expressed as follows:

$$J\ddot{\theta} = \tau_f + \tau_a + \tau_s + \tau_r + \tau_{gravity} + \tau_h + \tau, \tag{1}$$

where τ_f is the sum of the viscous and the solid friction. τ_s is the stiffness torque, τ_a, τ_r and $\tau_{gravity}$ are the acceleration, ground reaction forces and the gravity induced torques respectively. τ_h is the torque produced by the human muscles spanning the ankle joint. τ is the assistive torque provided by the orthosis. The torques mentioned above are considered positive when they cause dorsiflexion of the ankle joint. These torques can be expressed as follows:

$$\begin{aligned}
\tau_f &= -Asign(\dot{\theta}) - B\dot{\theta} \\
\tau_a &= -C(a_y cos(\alpha) - a_x sin(\alpha)) \\
\tau_s &= -K(\theta - \theta_r) \\
\tau_r &= -\gamma(R_1 x_1 - R_2 x_2 - R_3 x_3) cos(\alpha) \\
\tau_{gravity} &= -\tau_g cos(\alpha),
\end{aligned} \tag{2}$$

where θ_r is the ankle joint angle at the rest position of the foot. a_x and a_y are the foot's horizontal and vertical accelerations measured in the global frame. $R_i, i \in \{1, 2, 3\}$, represent the ground reaction force signals obtained from three force-sensitive resistors (FSRs) embedded in the insole of the left foot. These FSRs are optimally positioned at three key locations: the heel, the first toe, and the middle of the foot. $x_i, i \in \{1, 2, 3\}$, are the respective distances between each FSR and the ankle joint. A, B, C, K, γ and τ_g are respectively the solid and viscous friction, the acceleration, the stiffness, the ground reaction and the gravity torque coefficients.

III. Active disturbance rejection adaptive controller

The AAFO-wearer system presented in (1) relies heavily on the parameters in (2), which, for model-based controllers, requires an identification process prior to the experiments. Such identification process is not very suitable for wearable robots that can be used by several wearers during the rehabilitation process. Hence, the parameters of each wearer must be identified separately, which can be time and effort consuming. In addition to the diversity of users, it is important to note that these parameters can also change during the course of the experiment as a result of muscular fatigue. To avoid the identification process, an adaptive controller is proposed to drive the actuated ankle foot orthosis to track an adaptively generated ankle joint trajectory. The system's parameters are estimated based on the tracking error to improve the tracking accuracy. Although such controller does not require any prior identification, parameter estimation errors remain and can affect the system's performance. The parameter estimation errors alongside with the human muscular torque are estimated first using an adaptive extended state observer to be later on compensated in the control law, as shown in Fig. 2.

A. External torque estimation

The external torques exerted on the AAFO-wearer system are treated as an extended state and estimated using an extended state observer (ESO). To optimize the convergence speed of the estimated external input, it is advantageous to incorporate the known system information into the design of the extended state observer (ESO) [12]. For this specific case, the design of the observer will rely on the estimated system computed using an adaptive law. To ensure the comfort and the safety of the wearer while being assisted, it is crucial that the external input estimation be as smooth as possible. It is important to note that the estimated value will be used in the control law. Therefore, any excessive overshoot or chattering can have unpredictable effects on the wearer's balance, potentially increasing the risk of falling or injury. Hence, time-varying adaptive gains are used in a way to secure a smooth estimation and improve the accuracy.

Let $W \in \mathbb{R}^{1\times 6}$ be the vector of the AAFO-wearer system's parameters given by:

$$W = [\ A, B, C, K, \gamma, \tau_g\ ], \tag{3}$$

IEEE Robotics and Automation Letters (RA-L) paper, presented at ICRA 2024, Yokohama, Japan. Cite as RA-L paper.

IEEE Robotics and Automation Letters (RA-L) paper, presented at ICRA 2024, Yokohama, Japan. Cite as RA-L paper.

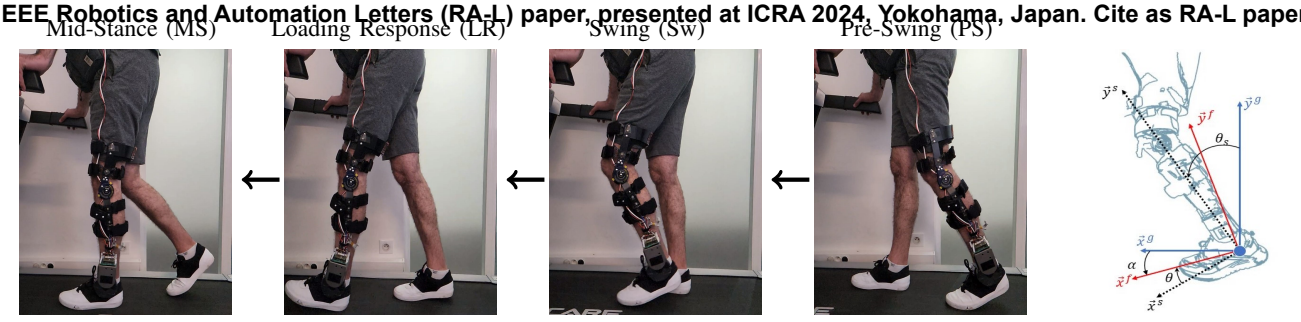

(a) (b) (c) (d) (e)

Fig. 1: Sub-figures (a), (b), (c), and (d) show snapshots of a subject wearing the AAFO while walking, the sequence of the gait cycle subphases is shown by the black arrows. On the right, sub-figure (e) represents the corresponding frames and angles used in the AAFO-wearer system model.

and $Y \in \mathbb{R}^{1\times 6}$ the corresponding vector of externally measured signals defined as:

$$Y = [\ sign(\dot{\theta}),\ \dot{\theta},\ a_y cos(\alpha) - a_x sin(\alpha),\ (\theta - \theta_r),\\ (R_1x_1 - R_2x_2 - R_3x_3)cos(\alpha),\ cos(\alpha)\ ]. \tag{4}$$

Thus, equation (1) can be written as:

$$\underbrace{J\ddot{\theta} + WY^T}_{f(\theta,\dot{\theta},\ddot{\theta})} = \tau + \tau_h \tag{5}$$

Consider the estimated dynamics based on the estimated parameters of the system as:

$$\hat{f}(\theta,\dot{\theta},\ddot{\theta}) = \hat{J}\ddot{\theta} + \hat{W}Y^T \tag{6}$$

Equation (5) can be written as the sum of the estimated dynamics $\hat{f}$ and the estimation error $\tilde{f}$:

$$f(\theta,\dot{\theta},\ddot{\theta}) = \hat{f}(\theta,\dot{\theta},\ddot{\theta}) + \tilde{f}(\theta,\dot{\theta},\ddot{\theta}) \tag{7}$$

For the sake of simplicity, the embedded parameters of the functions $f, \hat{f}$ and $\tilde{f}$ are removed in the sequel. As a result, the estimated dynamics can be written as:

$$\hat{J}\ddot{\theta} + \hat{W}Y^T = \tau + \hat{J}D \tag{8}$$

where

$$D = \hat{J}^{-1}(\tau_h - \tilde{f}) \tag{9}$$

is the resultant of the external torques affecting the estimated AAFO-wearer model.
Consider $x_1 = \theta, x_2 = \dot{\theta}$ and $x_3 = D$, equation (8) becomes:

$$\begin{cases} \dot{x}_1 = x_2 \\ \dot{x}_2 = -\hat{J}^{-1}\hat{W}Y^T + \hat{J}^{-1}\tau + x_3 \\ \dot{x}_3 = \dot{D} \end{cases} \tag{10}$$

Remark 1. *The human muscular torque τ_h developed at the ankle joint level is bounded by $\Delta_h : |\tau_h| \leq \Delta_h$.*

Assumption 1. *The external torque D affecting the estimated AAFO system model is considered to be bounded up to its first derivative, i.e. $|D| < B_D$ and $|\dot{D}| < B_{\dot{D}}$.*

The Adaptive Extended State Observer (AESO) used to estimated the external torque D is proposed as follows:

$$\begin{cases} \dot{\hat{x}}_1 = \hat{x}_2 + L_1\tilde{x}_1 \\ \dot{\hat{x}}_2 = -\hat{J}^{-1}\hat{W}Y^T + \hat{J}^{-1}\tau + \hat{x}_3 + L_2\tilde{x}_2 \\ \dot{\hat{x}}_3 = L_2L_3\tilde{x}_2 - \dot{L}_3L_1\tilde{x}_1 \end{cases} \tag{11}$$

where $\hat{x}_i$ is the estimation of x_i and the estimation error $\tilde{x}_i = x_i - \hat{x}_i, i \in \{1,2,3\}$. L_1 and L_2 are the first two adaptive gains proposed as:

$$\begin{cases} L_1(\tilde{x}_1) = a_1\ tanh\ (b_1\tilde{x}_1^2) \\ L_2(\tilde{x}_2) = a_2\ tanh\ (b_2\tilde{x}_2^2) \end{cases} \tag{12}$$

with $a_j, b_j \in \mathbb{R}^+, j \in \{1,2\}$. The ankle joint angle estimation error $\tilde{x}_1$ is computed as the difference between the ankle joint angle measured by the AAFO encoder and its estimation in (11). The angular velocity estimation error $\tilde{x}_2$ is computed as the difference between the angular velocity derived from the ankle joint angle measurement and its estimation in (11). L_3 is the third adaptive gain proposed as:

$$\dot{L}_3 = \begin{cases} c & \text{if } |\tilde{x}_2| \geq l \\ 0 & \text{otherwise} \end{cases} \tag{13}$$

where l and c are tuneable positive constants.

Proposition 1. *Consider the AAFO-wearer system model defined in* (5) *and its estimation given in* (8) *subjected to bounded external inputs $|D| \leq B_D$ and $|\dot{D}| \leq B_{\dot{D}}$ (Assumption 1). By considering the adaptive gains as proposed in* (12) *and* (13)*, the adaptive extended state observer in* (11) *ensures that the state estimation errors remain ultimately bounded.*

Proof. Based on (10) and (11), the estimation error dynamics are given by:

$$\begin{cases} \dot{\tilde{x}}_1 = \tilde{x}_2 - L_1\tilde{x}_1 \\ \dot{\tilde{x}}_2 = \tilde{x}_3 - L_2\tilde{x}_2 \\ \dot{\tilde{x}}_3 = \dot{D} - L_2L_3\tilde{x}_2 + \dot{L}_3L_1\tilde{x}_1 \end{cases} \tag{14}$$

Which can be represented in a matrix form as:

$$\underbrace{\begin{bmatrix} \dot{\tilde{x}}_1 \\ \dot{\tilde{x}}_2 \\ \dot{\tilde{x}}_3 \end{bmatrix}}_{\dot{\tilde{x}}} = \underbrace{\begin{bmatrix} -L_1 & 1 & 0 \\ 0 & -L_2 & 1 \\ \dot{L}_3L_1 & -L_3L_2 & 0 \end{bmatrix}}_{A} \underbrace{\begin{bmatrix} \tilde{x}_1 \\ \tilde{x}_2 \\ \tilde{x}_3 \end{bmatrix}}_{\tilde{x}} + \underbrace{\begin{bmatrix} 0 \\ 0 \\ 1 \end{bmatrix}}_{B} \dot{D} \tag{15}$$

where $\tilde{x}$ is the state estimation error vector. The characteristic polynomial for A is given by:

$$P(\lambda) = \lambda^3 + \lambda^2(L_1 + L_2) + \lambda L_2(L_1 + L_3) + L_1(L_2L_3 - \dot{L}_3) \tag{16}$$

For $\tilde{x}_1, \tilde{x}_2 \neq 0$ and by choosing the tuning parameters such that $L_{3_0} > 0$ and $a_2 \tanh(b_2 l^2)L_{3_0} - c > 0$, $P(\lambda)$ becomes

IEEE Robotics and Automation Letters (RA-L) paper, presented at ICRA 2024, Yokohama, Japan. Cite as RA-L paper.

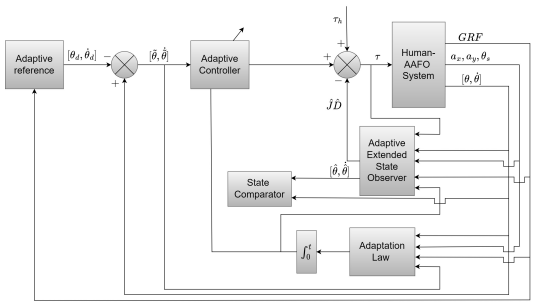

Fig. 2: Block diagram of the proposed AADRC strategy using an adaptive extended state observer and an adaptive controller to track an adaptively generated reference trajectory.

a third order polynomial with strictly positive coefficients, which has negative real part roots according to Routh-Hurwitz criterion. Consider the Lyapunov function:

$$T = \frac{1}{2}\tilde{x}^T\tilde{x} \tag{17}$$

Thus, for $0 < m < 1$, the derivative of T is given by:

$$\begin{aligned}\dot{T} &= \tilde{x}^T A\tilde{x} + \tilde{x}^T B\dot{D} \\ &\leq \lambda_{\max}(A)\|\tilde{x}\|^2 + \|\tilde{x}\|B_{\dot{D}} \\ &\leq \lambda_{\max}(A)(1-m)\|\tilde{x}\|^2 + \lambda_{\max}(A)m\|\tilde{x}\|^2 + \|\tilde{x}\|B_{\dot{D}}\end{aligned} \tag{18}$$

Note that A is a Hurwitz matrix with negative eigenvalues, i.e. $\lambda_{\max}(A) < 0$ where $\lambda_{\max}(A)(\cdot)$ is the highest eigenvalue of the embedded matrix. Therefore:

$$\dot{T} \leq \lambda_{\max}(A)(1-m)\|\tilde{x}\|^2 \quad \forall\|\tilde{x}\| \geq \frac{B_{\dot{D}}}{m|\lambda_{\max}(A)|} \tag{19}$$

$\dot{T} < 0$ outside the set $\{\|\tilde{x}\| \leq \rho\}$ where $\rho = \frac{B_{\dot{D}}}{m|\lambda_{\max}(A)|}$. Considering $T_M > \frac{1}{2}\rho^2$, solutions starting in the set $\{T \leq T_M\}$ will remain therein for all future time since $\dot{T} < 0$ on the boundary $T = T_M$. Therefore, the solutions are uniformly bounded for any ϵ such that $\frac{1}{2}\rho^2 < \epsilon < T_M$. $\dot{T} < 0$ in the set $\{\epsilon < T < T_M\}$ which means that T will decrease monotically until the solution enters the set $\{T < \epsilon\}$ where it cannot leave. Thus, the solution is uniformly ultimately bounded with the ultimate bound equal to $\sqrt{2\epsilon}$.

B. Adaptive Active Disturbance Rejection Controller □

In this section, the proposed adaptive active disturbance rejection controller (AADRC) is introduced. Additionally, the stability analysis of the AAFO-wearer system under the proposed adaptive controller and adaptive extended state observer is conducted.

Define first $s = \dot{\tilde{\theta}} + \lambda\tilde{\theta}$ where $\tilde{\theta} = \theta - \theta_d$, $\dot{\tilde{\theta}} = \dot{\theta} - \dot{\theta}_d$ and λ is a positive parameter. Define also $W_e = [W \quad J] \in \mathbb{R}^{1\times 7}$ as the extended vector that contains all the system's parameters, and $Y_e = [Y \quad (\ddot{\theta}_d - \lambda\dot{\tilde{\theta}})] \in \mathbb{R}^{1\times 7}$ the corresponding extended vector of externally measured signals.

Assumption 2. *The current and the desired ankle joint angles and their derivatives up to the second order $(\theta, \dot{\theta}, \ddot{\theta}, \theta_d, \dot{\theta}_d, \ddot{\theta}_d)$ are considered to be known and bounded.*

The proposed adaptive active disturbance rejection control torque has the following expression:

$$\tau = \hat{W}_e Y_e^T - ks - \hat{J}\hat{D} \tag{20}$$

where k is a positive gain and $\hat{D}$ is the estimated external input by (11). The parameter adaptation law is given by:

$$\dot{\hat{W}}_e^T = -\Gamma\ Y_e^T s \tag{21}$$

where $\Gamma = \text{diag}(\Gamma_i), i \in \{1, ..., 7\}$ is a positive definite scaling diagonal matrix.

Remark 2. *Note that the parameters estimated through* (21) *do not represent their true corresponding values. They are estimated to compute the assistive torque in a way to ensure the best possible trajectory tracking.*

Remark 3. *Consider the tracking error vector $X = [\tilde{\theta} \quad \dot{\tilde{\theta}}]^T$. $\hat{W}_e(t, X)$ and $\dot{\hat{W}}_e(t, X)$ are continuous functions, then $\frac{\partial \hat{W}_e}{\partial X}(t, X)$ with $\dot{\hat{W}}_e = \frac{\partial \hat{W}_e}{\partial X}\dot{X}$ is also continuous. Thus, by considering Assumption 2 and the parameter adaptation law* (21)*, $\dot{X}$ and $\dot{\hat{W}}_e$ are bounded. One concludes that $\frac{\partial \hat{W}_e}{\partial X}$ is also bounded. Hence, $\hat{W}_e(t, X)$ is Lipschitz in X [15], which implies that for any X_1 and X_2, $\|W_e(t, X_1) - W_e(t, X_2)\| \leq L\|X_1 - X_2\|$ where L is the Lipschitz constant. Therefore, for any bounded value of the tracking error vector X the estimated parameters vector $\hat{W}_e(t, X)$ is bounded, i.e, $\|\hat{W}_e\| \leq B_W$. Consequently, by considering Remark 1 alongside with Assumption 1 and* (9)*, the dynamical estimation error $\tilde{f}$ is bounded, i.e, $|\tilde{f}| \leq B_{\tilde{f}}$.*

Applying the adaptive control torque (20) to the AAFO system modeled by (1), the dynamics of the closed loop system can be expressed as follows:

$$J\dot{s} = -\tilde{W}_e Y_e^T - ks + \tau_h - \hat{J}\hat{D} \tag{22}$$

where $\tilde{W}_e = W_e - \hat{W}_e$. Equation (22) is equivalent to:

$$J\dot{s} = -\tilde{W}_e Y_e^T - ks + \hat{J}\tilde{D} + \tilde{f} \tag{23}$$

Proposition 2. *Consider the AAFO system modeled by* (1)*, subjected to the torques described in* (2) *and a bounded human torque (Remark 1). Under the assumption that the current and desired ankle joint angles and their derivatives up to the second order are bounded (Assumption 2), the control torque proposed in* (20) *with the parameter adaptation law in* (21) *and the external inputs estimated by the AESO in* (11) *ensures that the trajectories of the system $X = [\tilde{\theta}, \dot{\tilde{\theta}}]^T = [0, 0]^T$ remain uniformly ultimately bounded.*

Proof. Consider the Lyapunov function:

$$V = \frac{1}{2}Js^2 + \frac{1}{2}\tilde{W}_e\Gamma^{-1}\tilde{W}_e^T + k\lambda\tilde{\theta}^2 \tag{24}$$

Note that the system's parameters $(A, B, C, K, \gamma, \tau_g$ and $J)$ are considered to be constant, for a given subject, for this study. Consequently, the derivative of the Lyapunov function is:

$$\dot{V} = sJ\dot{s} - \tilde{W}_e\Gamma^{-1}\dot{\hat{W}}_e^T + 2k\lambda\tilde{\theta}\dot{\tilde{\theta}} \tag{25}$$

By replacing (21) and (23) in (25), the derivative of V becomes:

$$\begin{aligned}\dot{V} &= -k\dot{\tilde{\theta}}^2 - k\lambda^2\tilde{\theta}^2 + (\hat{J}\tilde{D} + \tilde{f})s \\ &= -kX^T\Lambda X + (\hat{J}\tilde{D} + \tilde{f})\Delta X\end{aligned} \tag{26}$$

IEEE Robotics and Automation Letters (RA-L) paper, presented at ICRA 2024, Yokohama, Japan. Cite as RA-L paper.

IEEE Robotics and Automation Letters (RA-L) paper, presented at ICRA 2024, Yokohama, Japan. Cite as RA-L paper.

where

$$\Lambda = \begin{bmatrix} \lambda^2 & 0 \\ 0 & 1 \end{bmatrix} \quad \text{and} \quad \Delta = \begin{bmatrix} \lambda & 1 \end{bmatrix}.$$

Consequently, for $0 < m < 1$, (26) becomes:

$$\begin{aligned} \dot{V} \leq & -k(1-m)\lambda_{\min}(\Lambda)\|X\|^2 - k\ m\ \lambda_{\min}(\Lambda)\|X\|^2 \\ & + |\hat{J}\tilde{D} + \tilde{f}|\sqrt{1+\lambda^2}\|X\| \end{aligned} \tag{27}$$

and therefore:

$$\dot{V} \leq -k(1-m)\lambda_{\min}(\Lambda)\|X\|^2 \quad \forall \|X\| \geq \frac{|\hat{J}\tilde{D} + \tilde{f}|\sqrt{1+\lambda^2}}{k\ m\ \lambda_{\min}(\Lambda)} \tag{28}$$

$\|X\|$ is bounded by μ, where $\mu = \frac{(B_W\sqrt{2\epsilon}+B_{\tilde{f}})\sqrt{1+\lambda^2}}{k\ m\lambda_{\min}(\Lambda)}$, where B_W and $B_{\tilde{f}}$ were defined in Remark 3.

From (24), the Lyapunov function V can be bounded by:

$$V \leq \alpha_1\|X\|^2 + \alpha_2$$

where $\alpha_1 = \frac{1}{2}J(1+\lambda^2)+k\lambda$ and $\alpha_2 = \frac{1}{2}\lambda_{\max}(\Gamma^{-1})(\|W_e\|+B_W)^2$. Choosing $c > \eta$ where $\eta = \alpha_1\mu^2 + \alpha_2$, the derivative of the Lyapunov function is negative on the boundary $V = c$. The solutions starting in the set $\{V \leq c\}$ will remain therein for all future time. For any set ϕ such that $\eta < \phi < c$, $\dot{V} < 0$ in the set $\{\phi < V < c\}$ thus V will decrease monotonically until the solutions enter the set $\{V \leq \phi\}$ and cannot leave it since $\dot{V} < 0$ on the boundary $V = c$. Therefore, the solutions are uniformly ultimately bounded. □

IV. Results

A. Simulation Results

To validate the accuracy of the external torque estimation performed by the proposed observer, numerical simulations were conducted to simulate a walking scenario on a treadmill. The required signals, including accelerations, ground reaction forces (GRF), shank angle, and reference trajectory, were initially recorded for a subject using the setup described in Section IV-B. The human torque τ_h was subsequently computed using the inverse dynamics of equation (1), with the control torque τ set to 0. To replicate the need for assistance, only 75% of the calculated τ_h was taken into account. Additionally, during the swing phase, τ_h was disregarded to simulate the FD effect. Fig. 3 shows the estimation accuracy of the proposed AESO where the root mean squared errors are $0.0893°$, $1.2837°/s$ and 0.2497Nm for the ankle joint angle, the angular velocity and the estimated torque respectively.

The performance of the proposed control strategy is evaluated and compared through simulations with state-of-the-art controllers such as the adaptive controller (AC) used in [16] and the commonly known active disturbance rejection controller (ADRC) [17]. The AC can be implemented by removing the AESO from the proposed control law, whereas an equivalent controller to the ADRC is used where the adaptation is removed from the proposed AADRC to be noted as ks-ADRC. The control torque for the AC and the ks-ADRC are given as follows:

$$\begin{cases} \tau_{\text{AC}} = \hat{W}_e Y_e^T - ks \\ \tau_{\text{ks-ADRC}} = -ks - J_{id}\hat{u}, \end{cases} \tag{29}$$

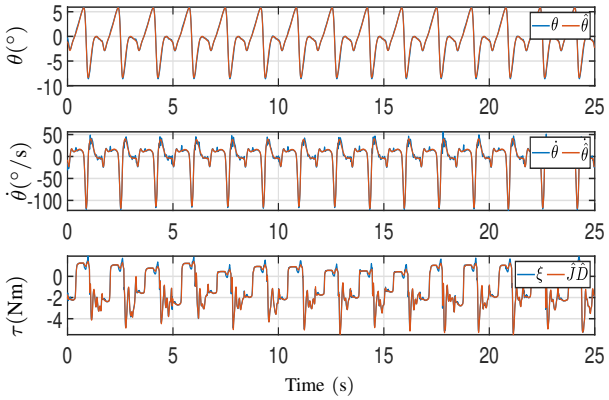

Fig. 3: Simulation results for the ankle joint angle, velocity and external torques estimation using the proposed AADRC. For all plots, the blue line shows the real state whereas the red line shows the estimated one.

where J_{id} is the identified value of J and $\hat{u}$ is the estimated external torque computed by (11) such that $\dot{\hat{x}}_2 = J_{id}^{-1}\tau + \hat{x}_3 + L_2\tilde{x}_2$. This ensures the same tuning for all controllers and provides a fair comparison. Table I shows the root mean squared tracking errors for the ankle joint angle and the angular velocity where the proposed controller is the best in terms of accuracy. This is due to its ability to adapt and provide the necessary assistance to complement the human muscular torque.

B. Experimental Setup

The AAFO is actuated by a DC motor connected to a gearbox, enabling control over the ankle joint angle. An incremental encoder measures the angle θ whereas the angular velocity $\dot{\theta}$ is numerically derived and filtered. The electronics and battery components are housed within a banana bag, which is securely fastened around the waist of the wearer (as depicted in Fig. 1). To measure the foot's three dimensional acceleration and the shank angle, two IMUs are mounted respectively on the foot and the shank of the left leg of the wearer. The ground reaction forces (GRF) are measured using three force-sensitive resistors (FSR) mounted in the shoe's insole at the heel, the first toe and the middle of the foot. Two electromyography (EMG) sensors are placed at the Tibialis Anterior (TA) and the Gastrocnemius Medialis (GM) muscles that are mainly responsible of the ankle joint dorsiflexion and plantarflexion, respectively.

C. Adaptive reference trajectory

The ankle joint reference profile was derived by averaging recorded gait cycles of 20 healthy subjects within a clinical setting, utilizing a motion capture system [18]. The gait ankle joint profile is generated adaptively to the walking speed using a set of three force sensitive resistors (FSR) mounted in each of the shoes' insoles. Interested readers are invited to refer to [16] for further details regarding the adaptive reference generation.

TABLE I: Root mean squared angle and angular velocity tracking errors calculated for different controllers through simulations.

Root Mean Squared Tracking Error			
	AC	ks-ADRC	AADRC
Angle (°)	1.7575	0.7892	0.2088
Angular Velocity (°/s)	8.4237	5.4738	2.8678

IEEE Robotics and Automation Letters (RA-L) paper, presented at ICRA 2024, Yokohama, Japan. Cite as RA-L paper.

IEEE Robotics and Automation Letters (RA-L) paper, presented at ICRA 2024, Yokohama, Japan. Cite as RA-L paper.

D. Experimental Protocol

During the experiments, the subjects were instructed to wear the AAFO and walk on a treadmill at a speed of 2 km/h. Each subject performed a series of three unassisted sessions followed by three assisted sessions for 90 seconds each. This sequential order was maintained consistently for all participants. In all the assisted sessions, the control strategy was initiated specifically during the stance phase of the gait cycle. This prevents sudden changes in the ankle joint that may affect the balance of the wearer. A one-minute rest period is allocated between each session to provide the subjects with an opportunity to recover and prepare for the subsequent session. This rest interval helps maintain the subjects' well-being and ensures the reliability of the experimental results. The experiments involved the participation of five healthy subjects noted A, B, C, D and E. Prior to the experiments, all subjects were thoroughly informed about the experimental protocols, and their written consent was obtained. The protocol was approved by local board from Henri Mondor Hospital. All necessary precautions were implemented to ensure the wellbeing and health of the participants. Additionally, measures were taken to ensure the privacy and confidentiality of their personal information.

E. Experimental results

The tuning parameters of the controller were set to: $\lambda = 5, k = 0.9$, as for the adaptive parameter's gains, $\Gamma_1 = 1e-3, \Gamma_2 = 5e-4, \Gamma_3 = \Gamma_4 = 1e-4, \Gamma_5 = 1e-7, \Gamma_6 = 1e-3$ and $\Gamma_7 = 1e-5$. $\hat{J}$ was initialized at 0.01 whereas all the other adaptive parameters had 0 as initial value. As for the AESO, its corresponding parameters were the following: $a_1 = 500, b_1 = 100, a_2 = 200, b_2 = 50, c = 0.1, L_{3_0} = 1$ and the accuracy threshold was set to $l = 2°/\text{s}$. These values were obtained by trial and error ensuring a compromise between the tracking accuracy and the comfort of the wearer. The same tuning was used for all five subjects who participated in the experiments. The ankle joint angle at its rest position was set to $\theta_r = 0°$.

a) Experimental result analysis for subject D: The results of the experiments conducted with Subject D are presented. Fig. 4 shows the ankle joint angle and the angular velocity estimated values during the first 30 seconds of the conducted experimental session. While the estimated states, such as the ankle joint angle and angular velocity, are initially initialized at zero, a rapid convergence towards the actual states is observed.

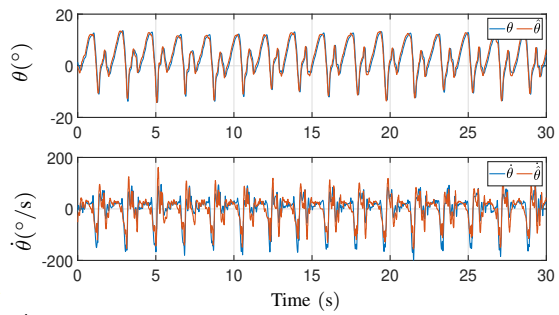

Fig. 4: Subject D: State estimation using the AESO showed during the first 30 seconds of the conducted experiment.

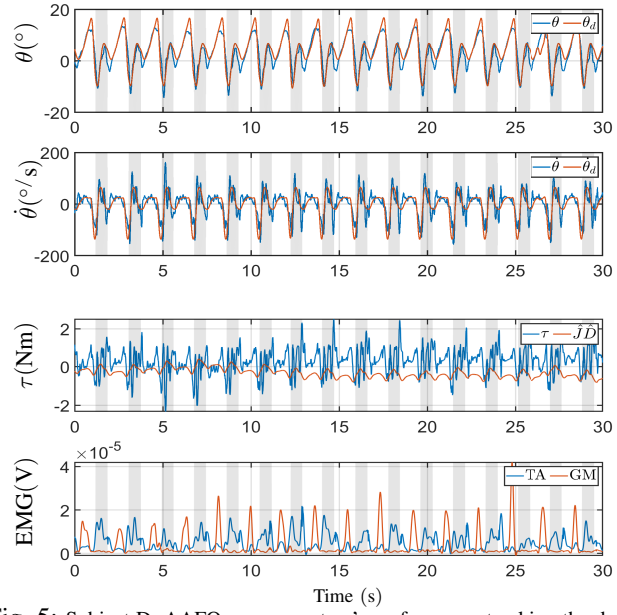

Fig. 5: Subject D: AAFO-wearer system's performance tracking the desired ankle joint angle profile during the first 30 seconds of the experiment. The first two plots show the angular position and the angular velocity tracking, while the third plot shows the assistive torque along side the estimation of the human muscular torque by the AESO. The bottom plot shows the EMG signals of the Tibialis Anterior (TA) and the Gastrocnemius Medialis (GM) muscles. For all plots, the shaded area represents the swing phase of the gait cycle.

The tracking performance for Subject D, where the AAFO is subject to the AADRC, is shown in Fig. 5. A positive torque provides dorsiflexion assistance, while a negative torque offers assistance in the plantarflexion direction. The estimated torque is observed to converge to its final value in approximately 12 seconds, which aligns well with the duration of the experiment. This convergence is reflected in the assistive torque, wherein during the initial transient phase of the session (i.e., the first 12 seconds), the torque progressively increases until it reaches a steady pattern. The evolution of the estimated human muscular torque aligns with the EMG signals of the Tibialis Anterior (TA) and the Gastrocnemius Medialis (GM) muscles. It can be seen that the estimated human muscular torque increases when the TA is activated (dorsiflexion) and decreases when the GM is activated (plantarflexion). This shows a good estimation trend of the human muscular torque by the AESO. The evolution of the estimated parameters for subject D is depicted in Fig. 6, demonstrating the convergence of the estimated parameters. It should be noted that these parameters do not

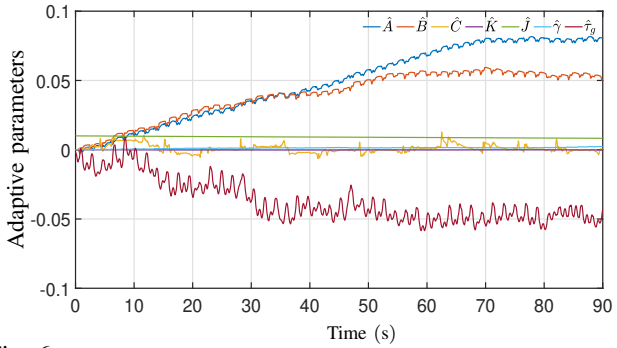

Fig. 6: Subject D: Estimated parameters of the AADRC during the assisted session showed during the first 90 seconds of the conducted experiment.

IEEE Robotics and Automation Letters (RA-L) paper, presented at ICRA 2024, Yokohama, Japan. Cite as RA-L paper.

IEEE Robotics and Automation Letters (RA-L) paper, presented at ICRA 2024, Yokohama, Japan. Cite as RA-L paper.

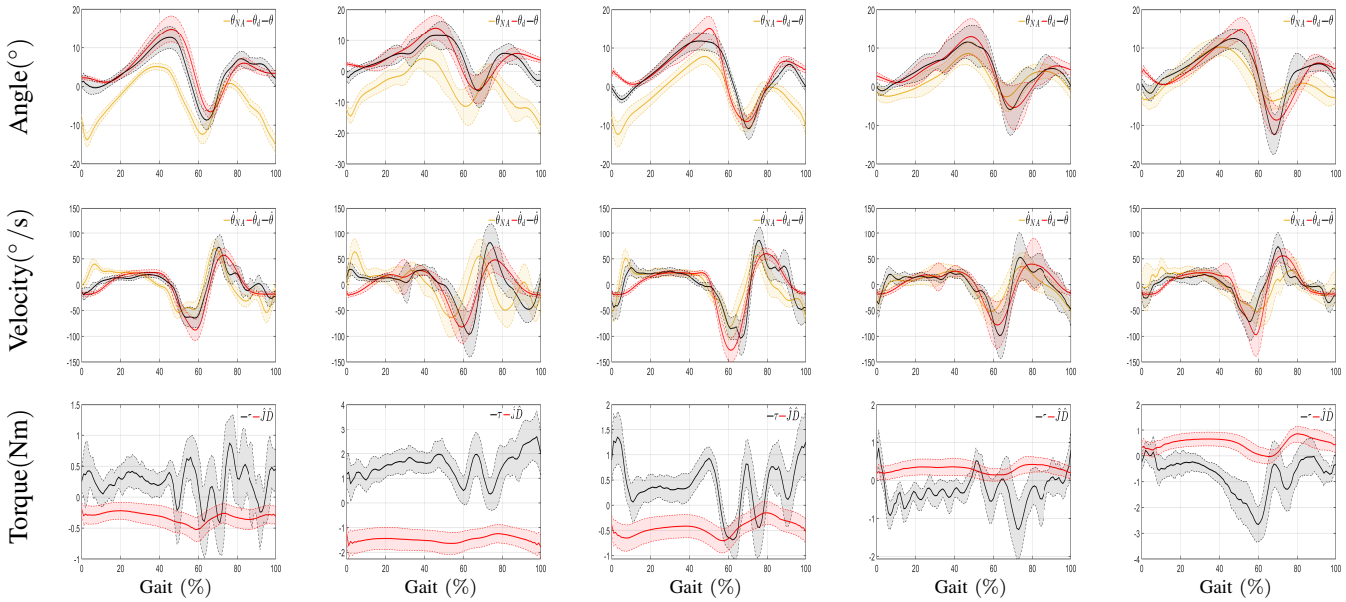

Fig. 7: Tracking performance and assistive torque for the five subjects using the proposed AADRC. The columns (a), (b), (c), (d) and (e) refer to the subjects A, B, C, D and E respectively. The top row presents the averaged ankle joint angle tracking and the middle row is the averaged ankle joint angular velocity tracking (red line: reference trajectory, black line: assisted gait, yellow line: unassisted gait). The bottom row shows the torques at the ankle joint level where the red line corresponds to the estimated external torques by the proposed AESO and the black line is the actual assistive torque developed by the proposed control strategy. For all plots, the dashed lines represent the standard deviation of the corresponding curve.

converge to a constant value, but to a bounded region due to the fact that the tracking error is proved to be bounded. It is also important to note that these parameters do not directly represent their true values (as mentioned in Remark 2). Instead, they are estimated based on the tracking error to achieve the best possible tracking performances.

b) Experimental result analysis for the five subjects: The performance of the AESO is shown for the five participants. Table II shows the average root mean squared estimation error of the ankle joint angle and the angular velocity calculated over all sessions. The estimation accuracy is seen through the relatively small error compared to the scale of the state.

To provide further insights into the assistance provided by the AADRC throughout the gait cycle, the evolution of the average ankle joint angle and angular velocity is depicted in Fig. 7 for both the assisted and the non-assisted cases. Additionally, the assistive torque and the estimated external torques are shown. The figures demonstrate that, for all subjects, the average ankle joint angle and angular velocity are synchronized with the reference trajectory. The average unassisted ankle joint angle of subjects A, B and C predominantly exhibits negative values, indicating a tendency to plantarflex their ankle joints. This is supported by the negative values of the estimated external torque, which represents a combination of the human muscular torque and the parameter estimation errors. Notably, for these subjects, the assistive torques are mostly positive throughout the gait cycle, providing assistance in the dorsiflexion direction to support in lifting the ankle joint angle towards the reference trajectory. On the other hand, for subjects D and E, the opposite pattern is observed and the assistance is provided mostly in the plantarflexion direction.

Table III shows a significant decrease in the EMG during the assisted sessions for the Tibialis Anterior (TA) and the Gastrocnemius Medialis (GM) muscles that are responsible for the dorsiflexion and the plantarflexion of the ankle joint respectively. Note that for subjects A, B and C, the EMG of the GM muscle decreased relative to the unassisted case by 18.31%, 11.28%, and 12.06% respectively, and by 4.52% and 2.19% for subjects D and E respectively. Notice that the decrease is significantly greater for subjects A, B and C.This refers to the tendency to plantarflex the ankle joint for these subjects, where the correction focused on shifting the ankle joint angle upward, thus, reducing the effort conducted by the GM muscle. Whereas for subjects D and E, the tendency to dorsiflex the ankle joint causes the unassisted ankle joint angle to be closer to the reference which explains the relatively small decrease in the EMG for the GM muscle.

Finally, the performance of the proposed AADRC is compared with 1) the non-assisted case (NA), then assisted cases where the assistance is provided by means of 2) the adaptive controller (AC), 3) the active disturbance rejection controller

TABLE II: Averaged root mean squared ankle joint angle and angular velocity estimation error values for the five subjects calculated over the sessions.

Ankle joint angle estimation error (°)				
A	B	C	D	E
1.98	1.626	1.7955	1.66	1.8954
Ankle joint angular velocity estimation error (°/s)				
A	B	C	D	E
9.65	18.36	17.77	15.9	25.48

TABLE III: Muscular EMG reduction (%) for the five subjects with respect to the unassisted case when using the proposed AADRC. TA; Tibialis Anterior, GM: Gastrocnemius Medialis.

Muscle	**EMG reduction (%)**				
	A	B	C	D	E
TA	22.41	16.51	27.36	26.72	18.37
GM	18.31	11.28	12.06	4.62	2.19

IEEE Robotics and Automation Letters (RA-L) paper, presented at ICRA 2024, Yokohama, Japan. Cite as RA-L paper.

TABLE IV: Comparison to state-of-the-art controllers : Average root mean squared angle and angular velocity tracking error.

Control	**Ankle joint angle tracking error** ($^\circ$)				
	A	B	C	D	E
NA	10.36	12.4	8.1923	6.435	4.9798
AC	4.39	5.1043	3.884	3.91	3.4152
ks-ADRC	3.9468	4.2353	3.0833	3.4	3.32
fg-ADRC	3.437	3.248	2.8355	3.2117	3.1495
AADRC	3.2	3.12	2.5418	2.674	3.0438
Control	**Ankle joint angular velocity tracking error** ($^\circ$/s)				
	A	B	C	D	E
NA	43	58.78	33.4139	25.83	33.6366
AC	32.8742	40.92	33.3272	23.9	31.9284
ks-ADRC	30.0425	34.6872	32.5162	23.23	30.3109
fg-ADRC	26.7	33.6125	30.8736	22.763	26.57
AADRC	19.05	32.1	30.2865	21.56	25.6990

(ks-ADRC), and 4) the fixed-gain active disturbance rejection (fg-ADRC) to show the effect of the adaptive gains used in AESO. The control torques for the AC and the ks-ADRC can be seen in (29). The fg-ADRC can be implemented by using fixed gains for the observer in the proposed AADRC. The tuning of these gains was performed using trial and error where they were increased until an unstable behavior in the estimation of the states was noticed. This ensures the best possible estimation accuracy. Table IV shows the average root mean squared angle and angular velocity tracking errors of the conducted experiments. At a first glance, one can notice a significant decrease in the tracking error when an assistance is applied. The AC had the worst tracking accuracy showing an average decrease of 47.52% in the tracking error with respect to the unassisted session. The ks-ADRC provided better tracking than the AC due to the rejection term added within the control law, showing an average decrease of 54% in the tracking error relative to the unassisted gait. The tracking was then improved when applying the fg-ADRC showing the importance of the adaptation law in the control torque where it presented an average decrease of 58.7% in the tracking error relative to the unassisted session. The best performance was obtained with AADRC highlighting the importance of the adaptive gains in the control torque and the estimator by showing an average decrease of 62% in the tracking error relative to the unassisted session. Note that the AESO showed better estimation of the AAFO-wearer system states compared to the fixed gain observer. This is due to the adaptive gains that can reach higher values than the fixed gains in the observer for a short duration without affecting the stability of the system.

V. Conclusions and Future Works

This paper introduces an adaptive active disturbance rejection control applied to an actuated ankle foot orthosis for assisting the ankle joint movement. An adaptive extended state observer is developed to estimate the external torque resulting form the human muscular torque and the unmodeled dynamics. The proposed AADRC computes adaptively the amount of assistance torque needed to perform a walking movement in complement to the human muscular effort. The experimental results showed a significant improvement in the ankle joint tracking when applying the proposed controller. Results showed also a superiority of the proposed controller with respect to adaptive controller or commonly used active disturbance rejection controller. The proposed approach can be extended to a full lower limb exoskeleton. However, it is essential to consider factors like kinematic coupling where the movement in one joint can affect the behavior of adjacent joints. In addition, the estimation of the human muscular torque at different levels of the exoskeleton can be challenging. Future works will focus on the validation of the proposed approach with foot-drop patients in clinical environment.

References

[1] Y. R. Mao, J. L. Zhao, M. J. Bian, W. L. A. Lo, Y. Leng, R. H. Bian, and D. F. Huang, "Spatiotemporal, kinematic and kinetic assessment of the effects of a foot drop stimulator for home-based rehabilitation of patients with chronic stroke: a randomized clinical trial," *Journal of NeuroEngineering and Rehabilitation*, vol. 19, no. 1, pp. 1–12, 2022.

[2] F. Alnajjar, R. Zaier, S. Khalid, and M. Gochoo, "Trends and technologies in rehabilitation of foot drop: a systematic review," *Expert Review of Medical Devices*, vol. 18, no. 1, pp. 31–46, 2021.

[3] C. Zhou, Z. Yang, K. Li, and X. Ye, "Research and development of ankle–foot orthoses: A review," *Sensors*, vol. 22, no. 17, p. 6596, 2022.

[4] G. York and S. Chakrabarty, "A survey on foot drop and functional electrical stimulation," *International Journal of Intelligent Robotics and Applications*, vol. 3, no. 1, pp. 4–10, 2019.

[5] A. Amerinatanzi, H. Zamanian, N. Moghaddam, A. Jahadakbar, and M. Elahinia, "Application of the superelastic NiTi spring in ankle foot orthosis (AFO) to create normal ankle joint behavior," *Bioengineering*, vol. 4, no. 4, p. 95, 2017.

[6] N. Gudapati, K. Kumaran, S. Deepak, R. Mukesh Kanna, R. Jinesh, and H. Poddar, "Design and control of a low-cost EMG-based soft robotic ankle-foot orthosis for foot drop rehabilitation," in *Machines, Mechanism and Robotics*. Springer, 2022, pp. 1367–1382.

[7] W. Huo, V. Arnez-Paniagua, G. Ding, Y. Amirat, and S. Mohammed, "Adaptive proxy-based controller of an active ankle foot orthosis to assist lower limb movements of paretic patients," *Robotica*, vol. 37, no. 12, pp. 2147–2164, 2019.

[8] R. Jradi, H. Rifai, Y. Amirat, and S. Mohammed, "Adaptive based assist-as-needed control strategy for ankle movement assistance," in *IEEE International Conference on Robotics and Automation (ICRA)*, 2023, pp. 12 672–12 678.

[9] H. Moon, R. Maiti, K. D. Sharma, Y. Amirat, P. Siarry, and S. Mohammed, "Hybrid half-gaussian selectively adaptive fuzzy control of an actuated ankle–foot orthosis," *IEEE Robotics and Automation Letters*, vol. 7, no. 4, pp. 9635–9642, 2022.

[10] J. Guerrero-Castellanos, H. Rifaï, V. Arnez-Paniagua, J. Linares-Flores, L. Saynes-Torres, and S. Mohammed, "Robust active disturbance rejection control via control lyapunov functions: Application to actuated-ankle–foot-orthosis," *Control Engineering Practice*, vol. 80, pp. 49–60, 2018.

[11] M. Zhang, J. Cao, S. Q. Xie, G. Zhu, X. Zeng, X. Huang, and Q. Xu, "A preliminary study on robot-assisted ankle rehabilitation for the treatment of drop foot," *Journal of Intelligent & Robotic Systems*, vol. 91, pp. 207–215, 2018.

[12] R. Madoński and P. Herman, "Survey on methods of increasing the efficiency of extended state disturbance observers," *ISA Transactions*, vol. 56, pp. 18–27, 2015.

[13] Y. Long, Z. Du, L. Cong, W. Wang, Z. Zhang, and W. Dong, "Active disturbance rejection control based human gait tracking for lower extremity rehabilitation exoskeleton," *ISA Transactions*, vol. 67, pp. 389–397, 2017.

[14] S. Aole, I. Elamvazuthi, L. Waghmare, B. Patre, and F. Meriaudeau, "Improved active disturbance rejection control for trajectory tracking control of lower limb robotic rehabilitation exoskeleton," *Sensors*, vol. 20, no. 13, p. 3681, 2020.

[15] H. K. Khalil, *Nonlinear systems; 3rd ed.* Upper Saddle River, NJ: Prentice-Hall, 2002.

[16] V. Arnez-Paniagua, H. Rifaï, Y. Amirat, M. Ghedira, J. Gracies, and S. Mohammed, "Adaptive control of an actuated ankle foot orthosis for paretic patients," *Control Engineering Practice*, vol. 90, pp. 207–220, 2019.

[17] J. Han, "From PID to active disturbance rejection control," *IEEE transactions on Industrial Electronics*, vol. 56, no. 3, pp. 900–906, 2009.

[18] E. Hutin, D. Pradon, F. Barbier, B. Bussel, J.-M. Gracies, and N. Roche, "Walking velocity and lower limb coordination in hemiparesis," *Gait & posture*, vol. 36, no. 2, pp. 205–211, 2012.